Available online at www.sciencedirect.com

SciVerse ScienceDirect

Ceramics International 38 (2012) 6335–6340

CERAMICS INTERNATIONAL

www.elsevier.com/locate/ceramint

Microstructure and mechanical properties of silicon carbide processed by Spark Plasma Sintering (SPS)

S. Hayun[a,*], V. Paris[b], R. Mitrani[a], S. Kalabukhov[a], M.P. Dariel[a], E. Zaretsky[b], N. Frage[a]

[a]*Department of Materials Engineering, Ben-Gurion University of the Negev, Beer-Sheva, Israel*
[b]*Department of Mechanical Engineering, Ben-Gurion University of the Negev, Beer-Sheva, Israel*

Received 27 March 2012; received in revised form 1 May 2012; accepted 1 May 2012
Available online 18 May 2012

Abstract

The unique combination of SiC properties opens the ways for a wide range of SiC-based industrial applications. Dense silicon carbide bodies (3.18 ± 0.01 g/cm^3) were obtained by an SPS treatment at 2050 °C for 10 min using a heating rate of 400 °C/min, under an applied pressure of 69 MPa. The microstructure consists of fine, equiaxed grains with an average grain size of 1.29 ± 0.65 μm. TEM analysis showed the presence of nano-size particles at the grain boundaries and at the triple-junctions, formed mainly from the impurities present in the starting silicon carbide powder. The HRTEM examination revealed high angle and clean grain boundaries. The measured static mechanical properties (H_V=32 GPa, E=440 GPa, σ_b=490 MPa and K_C 6.8 MPa m$^{0.5}$) and the Hugoniot Elastic Limit (HEL=18 GPa) are higher than those of hot-pressed silicon carbide samples.

Keywords: B. Microstructure; Dynamic mechanical proprieties; Spark Plasma Sintering (SPS); Silicon carbide

1. Introduction

Silicon Carbide (SiC) displays an unique combination of physical and mechanical properties, such as low density, oxidation resistance, strength retention at high temperature and high Hugoniot Elastic Limit (HEL) [1–5]. Such combination of properties makes it a choice material for a wide range of applications. It is difficult, however, to manufacture fully dense specimens by conventional sintering, on account of the elevated temperature required. The presence of sintering additives [2,6] may reduce the sintering temperature, but it detracts from the mechanical properties.

Spark Plasma Sintering (SPS) is a recent development in sintering technology that combines axial pressure with heating by an electrical current passing through the die that contains the powder body. This combination enhances significantly the sintering of covalently bonded refractory ceramics, such as boron and silicon carbides. Recently [7,8], we have investigated the microstructure and the mechanical properties (dynamic and static) of fully dense B_4C specimens that had been SPS-processed in the absence of any sintering additive. The SPS-processed B_4C samples displayed a higher level of physical and mechanical properties than those obtained by hot pressing. Several attempts to consolidate silicon carbide powder without additives by the SPS technology have been reported [9–12]. Guillard et al. [9] applied a one stage SPS procedure for synthesizing and densifying silicon carbide from a powder mixture of graphite and silicon. Using this procedure, a 92% Relative Density (RD) was achieved. Close to 98% RD was reported for specimens fabricated by SPS using silicon carbide nanopowder (~70 nm) [10] and from powder obtained by mechanical alloying [11,12]. The present work is a follow up of our investigation of the microstructure and mechanical properties (both static and dynamic) of the SPS-processed covalent ceramics.

2. Experimental procedure

2.1. Starting materials and experimental set-up

Silicon carbide powder UF 15 grade (Table 1), supplied by H.C. Starck Company was inserted into a graphite die

*Corresponding author. Tel.: +972 8 6461469; fax: +972 8 6489441.
E-mail address: shayun@bgu.ac.il (S. Hayun).

0272-8842/$36.00 © 2012 Published by Elsevier Ltd and Techna Group S.r.l.
http://dx.doi.org/10.1016/j.ceramint.2012.05.003

(inner diameter 20 mm, outer diameter 40 mm), which was covered with 20 mm thick graphite wool for thermal insulation. The die was placed to the SPS apparatus (type HP D5/1, FCT System. Rauenstein, Germany) equipped with a 50 kN uniaxial press [7]. Based on preliminary results, the SPS consolidation was conducted at 2050 °C under vacuum (1.3 h Pa) and uni-axial pressure of 69 MPa. The heating rate was 400 °C/min and the holding time at the sintering peak temperature varied from 0 to 10 min.

2.2. Microstructural characterization

The microstructure was studied using Scanning Electron Microscopy (SEM, JEOL-35) and by Transmission Electron Microscopy (TEM) JEOL FasTEM 2010 equipped with the Noran Energy Dispersive Spectrometer (EDS). The samples for the SEM characterization were prepared using a standard metallographic procedure finalized by polishing with a 1 μm diamond paste. Polished specimens were thermally etched for 1 h at 1200 °C under vacuum (1.3×10^{-4} h Pa). The TEM samples were prepared as follows: 1 mm thick foils were cut using a 0.4 mm diamond saw and ground down to 500 μm. Disks, 3 mm diameter, were drilled with a cooper drill pipe and 40 μm diamond paste, ground down to 70 μm thickness, glued to a Cu support and polished to 30 μm thickness. Final thinning to electron transparency was carried out with a Gatan^{TM} model 691 precision ion polishing system until foil perforation.

2.3. Static mechanical properties

The hardness of the SPS-processed silicon carbide samples was determined by a Buehler-Micromet 2100 microhardness tester with a Vickers indenter under 20 N loads. The flexural strength was determined by the three-point bending test on $3 \times 4 \times 20$ mm bars in an LRX Plus LLOYD instrument (Lloyd Instruments, Fareham Hants, UK). The velocities of the longitudinal C_l and shear C_s acoustic waves were measured by the pulse-echo technique using a 5 MHz probe. The elastic moduli were derived from the ultrasonic velocity data and the density values measured by the liquid displacement method in distilled water.

2.4. Dynamic behavior

In order to characterize the response of the material to dynamic (impact) loading, a series of planar impact experiments was carried out with a smooth bore 25-mm diameter, 6-meter long gas gun. The gun is capable of accelerating the PMMA projectile equipped with a 1–2 mm thick impactor to a velocity of about 1.2 km/s. The impactors were tungsten or copper (1.0–1.2 mm thickness), 24.5 mm diameter disks. The silicon carbide specimens were polished to ensure 5-μm parallelism of their surfaces. The reflectivity of the rear surface of the specimens was enhanced by a submicron thick layer of vapor-deposited gold. To prevent the loss of reflectivity caused by the arrival of the shock at the sample surface, 6-mm polymethylmetacrylate (PMMA) windows were glued on the coated rear surface. The velocity of the specimen–window interface was continuously monitored by a Velocity Interferometer System for Any Reflector (VISAR) [13].

3. Results and discussion

Evolution of the silicon carbide sintering behavior during the SPS process was carried out by using the densification curve and its derivative as a function of time (Fig. 1). The data presented in Fig. 1 corresponds to the process with 10 min holding time at the sintering temperature. Densification of silicon carbide powder starts at 1000 °C. The densification rate increases significantly at 1900 °C. At the peak sintering temperature, 2050 °C, the densification rate decreases and approaches zero after 10 min of soaking and the density reaches its maximum, RD 99.4%.Fig. 2 The microstructure of the dense specimens consists of fine equiaxed grains with an average grain size of 1.30 ± 0.65 μm, and a small amount of nano-size pores (Fig. 3). TEM analysis was performed (Fig. 4), in order to clarify the detailed characteristics of Grain Boundaries (GB), Sub-micron particles, composed mainly from Al, Fe and Ni, were observed at the GB and, at the triple-junctions, in particular, These particles are due to the impurities present in the original silicon carbide powder (Table 1). The HRTEM image, (Fig. 5) showed high-angle clean GB that were free of amorphous films in contrast to their presence in hot pressed silicon carbide[14,15].

3.1. Static mechanical properties

The hardness of the SPS processed silicon carbide changes from 20 ± 2 GPa to 32 ± 0.7 GPa with the relative density increasing from 89 to 99.4%. Young's modulus and the flexural strength of silicon carbide also increase as a function of the relative density (Fig. 5). The fully

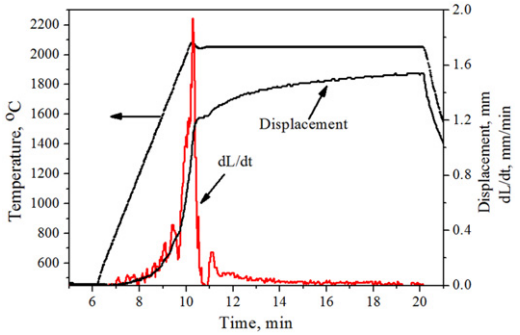

Fig. 1. Densification curve and its derivative (densification rate) as function of time of processing of silicon carbide specimen. During the whole sintering cycle, the sample was under 62 MPa axial pressure.

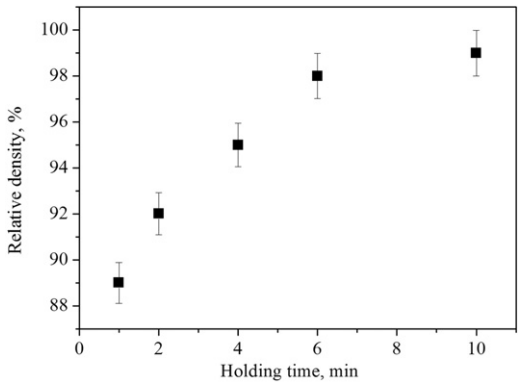

Fig. 2. Effect of holding time on the relative density of silicon carbide specimens.

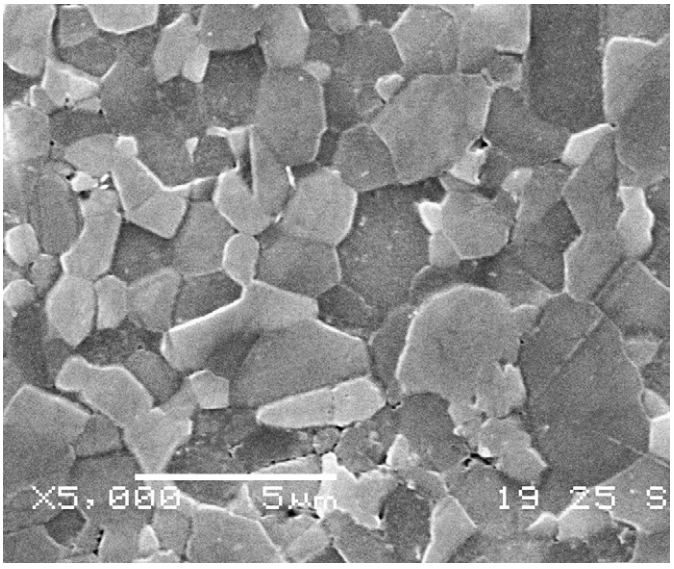

Fig. 3. SEM image of the SPS-processed silicon carbide specimen after thermal etching.

dense material displays high values of Young's modulus (440 ± 20 GPa) and the flexural strength (490 ± 70 MPa). These values are higher than those reported for hot-pressed silicon carbide [1,3]. As apparent from Fig. 6, the fracture mode of the presently studied silicon carbide is a mixture of intergranular and transgranular fracture.

The fracture toughness, K_C, was determined from the lengths of the cracks generated at the corners of the Vickers imprints [8,16–18]. The optical images of the indentation vicinity, after the indentation and after the subsequent polishing (Fig. 7), indicate that the cracks appearing under the indentation of the SPS processed silicon carbide correspond to a Palmqvist crack system [17,18]. The equations that have been put forward in [17,18] for such crack system yield K_C value of 6.9 ± 0.1 and 6.8 ± 0.1 MPa $m^{0.5}$, respectively. These values are higher than those reported in the literature for SiC-AlN ($\sim$3.25 MPa $m^{0.5}$) [19–21] and close to values for the SiC-YAG system ($\sim$6.35 MPa $m^{0.5}$) [22].

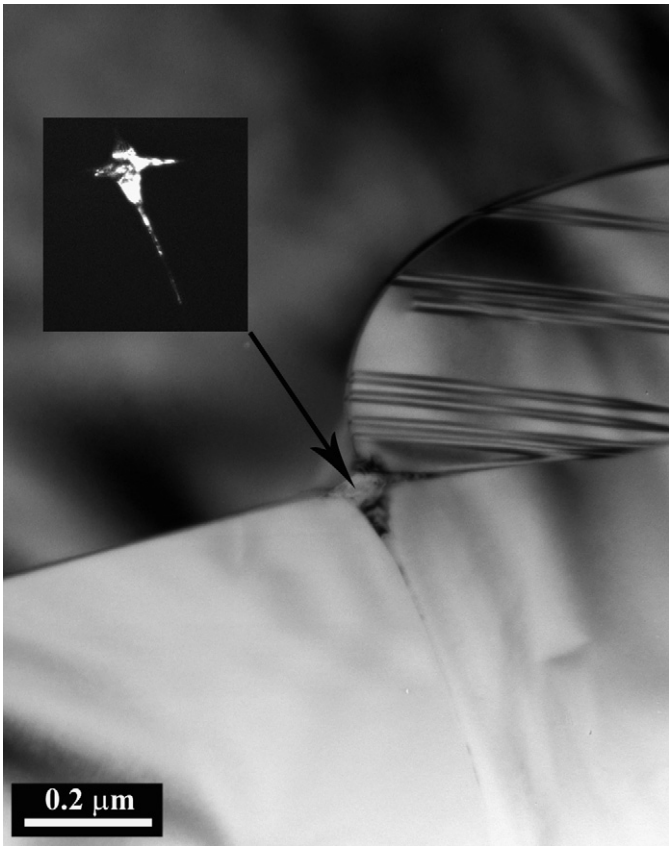

Fig. 4. Bright field TEM image of a triple junction of the grain boundaries in SPS processed silicon carbide. The inset is the dark field image of the impurity at the triple junction.

Table 1
Powder characteristics.

α-SiC Acheson type mainly 6H polytype		
Specific surface area		14–16 m^2/g
Particle size distribution	≤ 1.2 μm	D 90%
	≤ 0.55 μms	D 50%
	≤ 0.2 μm	D 10%
Impurity levels	O	1.5 wt%
	Al	0.03 wt%
	Ca	0.01 wt%
	Fe	0.03 wt%
Total carbon	C	29.0–30.0 wt%

3.2. Dynamic properties

The parameters of the planar impact experiments performed with porous and fully dense silicon carbide specimens are given in Table 2 together with the HEL values derived from the experimental results. Typical SiC/PMMA interface velocity histories $w_{if}(t)$ recorded after loading the fully dense and slightly porous (RD of about 97.5%) silicon carbide disks by W impactors are shown in Fig. 8. The interface velocity w_{if}^{HEL} (see Fig. 8) was used for

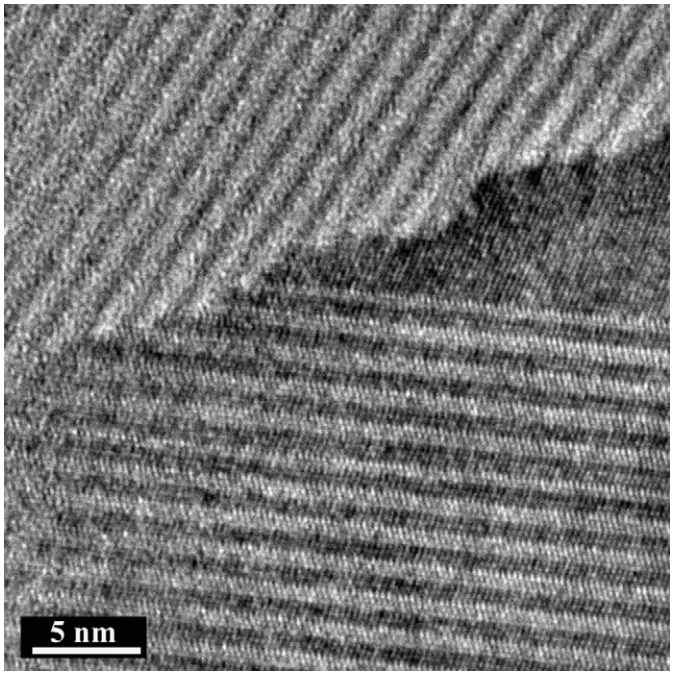

Fig. 5. Typical HRTEM images from the grain boundary of SPS processed silicon carbide.

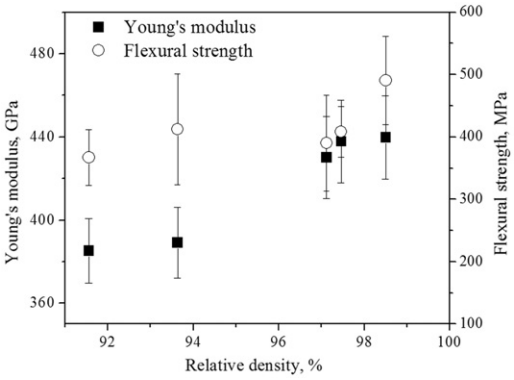

Fig. 6. Young's modulus and the hardness as a function of the measured relative density.

determination of the HEL value according to [23]:

$$\sigma_{\mathrm{HEL}} = \frac{1}{2} w_{if}^{\mathrm{HEL}} \left[(\rho C_l)_{\mathrm{Cer}} + (\rho D)_{\mathrm{PMMA}} \right] \quad (1)$$

where $(\rho_0 C_l)_{Cer}$ is the elastic impedance of the ceramic and $(\rho_0 D)_{PMMA}$ is the shock impedance of the PMMA window. The latter was derived from the PMMA data reported in [24]. The obtained HEL values (Table 2) for fully dense silicon carbide processed by SPS, along with the data reported in the literature [23–26] as a function of the grain size, are shown in Fig. 9. The HEL values for the SPS-processed silicon carbide, which displays a fine microstructure, are higher than those of hot-pressed specimens Fig. 10.

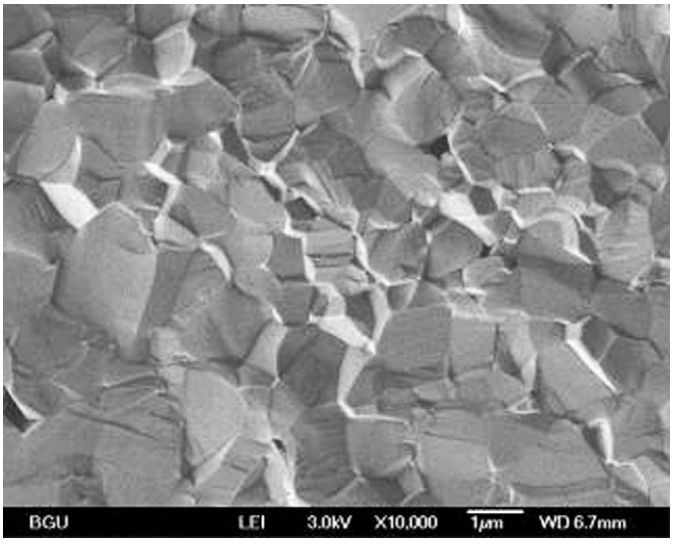

Fig. 7. SEM micrograph of the fracture surface of SPS processed silicon carbide with 99.7% relative density.

In order to evaluate the inelastic dynamic behavior of the SPS-processed silicon carbide, the correlation between the hardness (H_V) and compressive strength (Y) [28–30] $H_V/Y \approx 3$, is used. For dynamic experiments, Y is considered as the material failure threshold under 1-D stress compression.

Based on Griffith's brittle failure criterion, Rosenberg [31,32] proposed the relation:

$$Y_{br} = \frac{(1-2\nu)^2}{1-\nu} \sigma_{HEL}, \quad (2)$$

where σ_{HEL}, ν and Y_{br}, are HEL value, Poisson's ratio and the dynamic threshold stress corresponding to the onset of the brittle fracture in compression, respectively. Eq. (2) gives Y_{br} values ranging from 6.2 to 9.2 GPa. Taking into account the respective hardness values of fully dense (32 GPa) and porous (24.5 GPa) silicon carbide, the H_V/Y ratios were estimated as 3.50 and 3.95. If the equation $Y^{\mathrm{duct}} = ((1-2\nu)/(1-\nu))\sigma_{HEL}$, based on the von Mises criterion for ductile yielding is used, the H_V/Y ratio are equal to 2.22 and 2.53 for fully dense and porous material, respectively. Since the H_V/Y ratios calculated according to two different criteria are almost equally distant from the common value of 3, we are unable to derive an unambiguous conclusion concerning the mode, either brittle or ductile, of the inelastic deformation in the SPS-processed silicon carbide above its HEL. It is believed, however, that in the presence of some porosity, the collapse of the pores dictates the post HEL response of porous silicon carbide specimens.

4. Summary

Fully dense silicon carbide specimens with fine equiaxed grains (average grain size is 1.28 ± 0.64 μm) were fabricated

Table 2
Parameters of planar impact tests and dynamic properties of SiC specimens.

Test	Impact velocity (km/s)	Impactor material	Impactor/target thickness (mm)	Density (g/cm^3)	Cl (km/s)	Cb (km/s)	σ_{HEL} (GPa)	YD (GPa) (Griffith)	YD (GPa) (von Mises)
SiCA	1.0	W	1.06/2.50	3.204	12.67	8.80	18.5	9.2	14.4
SiCB	1.1	Cu	1.00/2.69	3.203	12.73	8.91	17.6	8.5	13.7
SiCE	0.68	W	1.18/5.00	3.130	12.28	8.51	12.4	6.2	9.7
SiCF	1.05	W	1.19/4.96	3.124	12.19	8.37	13.2	6.9	10.4

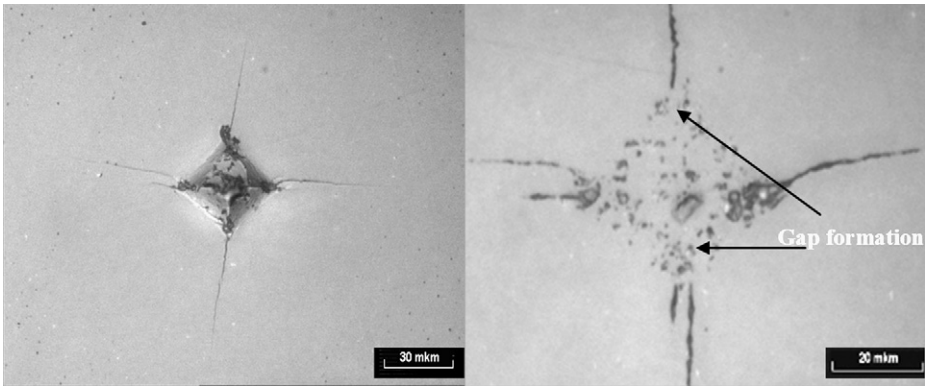

Fig. 8. Optical images of a Vickers imprint just after the indentation (a), and after the subsequent polishing (b). The right image shows the presence of the bulk material between the crack and the imprint indicating the Palmqvist cracks.

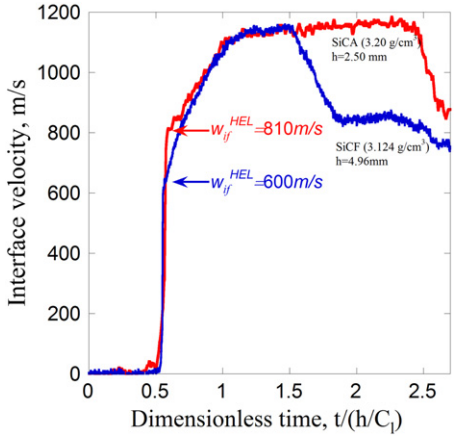

Fig. 9. SiC/PMMA interface velocity histories recorded in the plate impact tests listed in Table 2. In order to account for the difference of the samples thickness the time is normalized on the period of the reverberating of the elastic wave in the sample of thickness h.

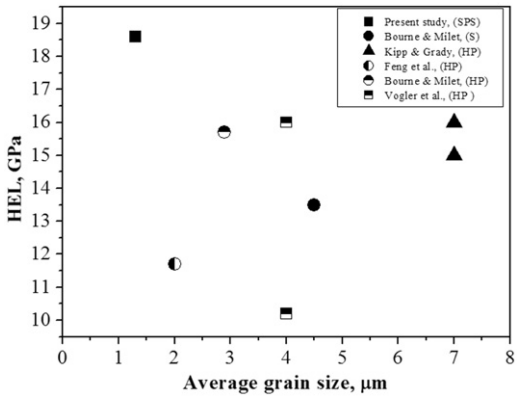

Fig. 10. Stress at HEL as a function of the grain size of silicon carbides [4,25–27]. For clarity, only the maximum and minimum HEL values of each study are shown.

by SPS technology at 2050 °C in the absence of sintering additives. The TEM analysis discerned the presence of the inclusions of the secondary phases at the triple grain junctions and GB, which originated from impurities in the starting silicon carbide powder. The HRTEM observation did not reveal any amorphous layer at the grain boundaries. The fully dense silicon carbide displays high fracture toughness (6.8 MPa m$^{0.5}$), Young's modulus (440 GPa), flexural strength (490 MPa) and hardness (32 GPa). The value of HEL of the fully dense specimens (18 GPa) is higher than that of the hot-pressed silicon carbide with similar grain size; while for slightly porous (2.6% vol. porosity) specimens, it is much lower (13 GPa). Thus, the SPS-processed SiC ceramic is highly competitive with its hot-pressed counterpart.

Acknowledgment

This work was partially supported by the Ministry of Defense (Israel). The authors like to thank Dr. V. Ezersky for the TEM analysis.

References

[1] J.B. Wachtman, D.G. Lam, Young's modulus of various refractory materials as a function of temperature, Journal of the American Ceramic Society 42 (1959) 254–260.

[2] S. Baud, F. Thévenot, Microstructures and mechanical properties of liquid-phase sintered seeded silicon carbide, Materials Chemistry and Physics 67 (2001) 165–174.

[3] L.L. Snead, T. Nozawa, Y. Katoh, T. Byun, S. Kondoand, D.A. Petti, Handbook of SiC properties for fuel performance modeling, Journal of Nuclear Materials 371 (2007) 329–377.

[4] J.C.F. Millett, N.K. Bourneand, D.P. Dandekar, Delayed failure in a shock-loaded silicon carbide, Journal of Applied Physics 97 (2005) 113513.

[5] V.A. Izhevskyi, L.A. Genova, J.C. Bressianiand, A.H.A. Bressiani, Review article: silicon carbide. Structure, properties and processing,, Cerâmica 46 (2000) 4–13.

[6] J.H. She, K. Ueno, Effect of additive content on liquid-phase sintering on silicon carbide ceramics, Materials Research Bulletin 34 (1999) 1629–1636.

[7] S. Hayun, S. Kalabukhov, V. Ezersky, M.P. Darieland, N. Frage, Microstructural characterization of spark plasma sintered boron carbide ceramics, Ceramics International 36 (2010) 451–457.

[8] S. Hayun, V. Paris, M.P. Dariel, N. Frageand, E. Zaretzky, Static and dynamic mechanical properties of boron carbide processed by spark plasma sintering, Journal of the European Ceramic Society 29 (2009) 3395–3400.

[9] F. Guillard, A. Allemand, J. Lulewiczand, J. Galy, Densification of SiC by SPS-effects of time, temperature and pressure, Journal of the European Ceramic Society 27 (2007) 2725–2728.

[10] A. Maître, A.V. Put, J.P. Laval, S. Valetteand, G. Trolliard, Role of boron on the Spark Plasma Sintering of an α-SiC powder, Journal of the European Ceramic Society 28 (2008) 1881–1890.

[11] M. Ohyanagi, T. Yamamoto, H. Kitaura, Y. Kodera, T. Ishiiand, Z.A. Munir, Consolidation of nanostructured SiC with disorder–order transformation, Scripta Materialia 50 (2004) 111–114.

[12] T. Yamamoto, T. Kondou, Y. Kodera, T. Ishii, M. Ohyanagi, Z. Munir, Mechanical properties of β-SiC fabricated by spark plasma sintering, Journal of Materials Engineering and Performance 14 (2005) 460–466.

[13] L.M. Barker, R.E. Hollenbach, Laser interferometer for measuring high velocities of any reflecting surface, Journal of Applied Physics 43 (1972) 4669–4675.

[14] D.R. Clarke, High-temperature microstructure of a hot-pressed silicon nitride, Journal of the American Ceramic Society 72 (1989) 1604–1609.

[15] X.F. Zhang, M.E. Sixta, L.C. De Jonghe, Grain boundary evolution in hot-pressed ABC-SiC, Journal of the American Ceramic Society 83 (2000) 2813–2820.

[16] C. Ponton, R. Rawlings, Vickers indentation fracture-toughness test. 1. Review of literature and formulation of standardized indentation toughness equations, Materials Science and Technology 5 (1989) 865–872.

[17] K. Niihara, A fracture mechanics analysis of indentation-induced Palmqvist crack in ceramics, Journal of Materials Science Letters 2 (1983) 221–223.

[18] D.K. Shetty, I.G. Wright, P.N. Mincer, A.H. Clauer, Indentation fracture of WC-Co cermets, Journal of Materials Science 20 (1985) 1873–1882.

[19] H. Kodama, T. Miyoshi, Study of fracture behavior of very fine-grained silicon carbide ceramics, Journal of the American Ceramic Society 73 (1990) 3081–3086.

[20] S.K. Lee, C.H. Kim, Effects of-Sic versus-Sic starting powders on microstructure and fracture toughness of Sic sintered with Al2O3-Y2O3 Additives, Journal of the American Ceramic Society 77 (1994) 1655–1658.

[21] Y. Kim, J. Lee, Effect of polycarbosilane addition on mechanical properties of hot-pressed silicon carbide, Journal of Materials Science 27 (1992) 4746–4750.

[22] J. Kim, Y. Kim, M. Mitomo, G. Zhanand, J. Lee, Microstructure and mechanical properties of alpha-silicon carbide sintered with yttrium-aluminum garnet and silica, Journal of the American Ceramic Society 82 (1999) 441–444.

[23] G.I. Kanel, V.E. Fortov, S.V. Razorenov, Shock-Wave Phenomena and the Properties of Condensed Matter, Springer, New York, NY, 2004, pp. 322.

[24] S.P. Marsh, LASL Shock Hugoniot Data, University of California Press, Berkeley, 1980.

[25] D.E. Grady, Shock-wave strength properties of boron carbide and silicon carbide, Journal de Physique IV Proceedings 4 (1994) C8-385–C8-391.

[26] T. Sekine, T. Kobayashi, Shock compression of 6 H polytype SiC to 160 GPa, Physical Review B 55 (1997) 8034–8037.

[27] M. Kipp, D.E. Grady, Shock compression and release in high-strength ceramics, in: S.C. Schmidt, J.N. Johnson, L.W. Davison (Eds.), Shock Compression of Condensed Matter 1989, North-Holland, Amsterdam, 1990, pp. 377–380.

[28] J.J. Gilman, Relationship between impact yield stress and indentation hardness, Journal of Applied Physics 46 (1975) 1435–1436.

[29] J. Lankford, The compressive strength of strong ceramics: microplasticity versus microfracture, Journal of Hard Materials 2 (1991) 55–77.

[30] W.A. Dunlay, C.A. Tracy, P.J Perrone, A proposed uniaxial compression test for high strength ceramics, MTL TR 89-89, 1989.

[31] Z. Rosenberg, On the relation between the Hugoniot elastic limit and the yield strength of brittle materials, Journal of Applied Physics 74 (1993) 752–754.

[32] Z. Rosenberg, On the correlation between dynamic compressive strengths of strong ceramics and their indentation hardness, in:S.C. Schmidt, W.C. Tao (Eds.), Proceedings of the Conference of the American Physical Society Topical Group on Shock Compression of Condensed Matter, AIP, New York, 1996, pp. 543–546.